Paper:
Lesyuk, R., Lesnyak, V., Herguth, A., Popovych, D., Bobitski, Y., Klinke, C. & Gaponik, N. (2017). Simulation study of environmentally friendly quantum-dot-based photovoltaic windows. *Journal of Materials Chemistry C, 5*(45), 11790-11797.
http://dx.doi.org/10.1039/C7TC02945D

Simulation Study of Low-Toxic Quantum Dot Based Photovoltaic Windows

Rostyslav Lesyuk[1], Vladimir Lesnyak[2], Axel Herguth[3], Dmytro Popovych[4], Yaroslav Bobitski[5,6], Christian Klinke[1], Nikolai Gaponik[2] *

[1] Institute for Physical Chemistry, University of Hamburg, Grindelallee 117, 20146 Hamburg, Germany

[2] Physical Chemistry and Center for Advancing Electronics Dresden (cfAED), TU Dresden, Bergstr. 66b, 01062 Dresden, Germany

[3] Photovoltaic Division, Department of Physics, University of Konstanz, Universitätsstr. 10, 78457 Konstanz, Germany

[4] Pidstryhach Institute for applied problems of mechanics and mathematics of NAS of Ukraine (L'viv, Ukraine)

[5] Photonics Department, Lviv National Polytechnic University (Lviv, Ukraine)

[6] University of Rzeszow (Rzeszów, Poland)

* Corresponding author: nikolai.gaponik@chemie.tu-dresden.de.

Abstract We model a prototype of photovoltaic window, passive source of clean energy, by means of a Monte-Carlo ray tracing method. We consider different geometries, material properties and edge solar cells for the definition of optimal conditions and the possible electrical power yield. The modelled photovoltaic window prototype is based on colloidal luminescent low-toxic I-III-VI quantum dots (core/shell $CuInS_2$/ZnS nanocrystals) with large Stokes-shifts, high quantum yields and tunable spectral properties. We also show the influence of the quantum dots' absorption/emission spectra on the resulting spectrum of transmitted light (i.e. visual appearance of the photovoltaic window) using the chromaticity diagram.

Solar energy harvesting is a very promising way to guarantee the energy supply for the humanity in the XXI century. Nowadays, we observe a gradual and steady increase of the energy production from renewable resources. One of the most impetuous trends shows the photovoltaic (PV) energy sector. The installed capacity of PV solar plants and roof systems over the last decade increased by the factor 45 with an average annual increase of more than 46% [1, 2] and reached by the end of 2015 231 GW_p of the installed capacity producing 253 TWh of electrical energy annually (corresponds to 1.1% of the global electricity consumption).

However the growth rate of installed capacities slowed down in the last several years to 28% in 2015, the production of solar energy in turn to 32.6% (from 91% in 2011)[1, 3]. By keeping these growth rates, and by the balanced increase of the global electricity consumption by ~1% annually, the solar electricity production can essentially contribute to the electricity balance and even cover our global electricity needs by around 2035 (estimation based on ref. [1]). However, to retain these annual rates, e.g. in 2030 new solar plants with the area comparable to such countries as Qatar should be installed. To compensate the degradation of already installed PV capacities, this area should be even larger. Such rates are obviously not achievable by the nowadays level of technology and costs. Presumably, further slowing of solar energy growth will take place, and in this case the remarkable overlap of produced solar energy and consumed electricity will be shifted toward the far future. On the other hand, the increasing production of electrical vehicles may move the energy balance of the planet gradually further from oil and gas to the electricity sector, which at the moment is not able to cover these needs.

Breakthrough technologies including safe nuclear fusion, environmental friendly fuel cells, wind plants and low cost sunlight conversion are in focus of modern research and developments. In the 70s the concept of luminescent collectors (in the following luminescent solar concentrators, LSCs) was introduced [4, 5] as a potential way to the low cost solar energy, and vast analytical and experimental research has been done since, based mainly on application of dyes in LSCs [6-9]. In order to improve the performance of LSCs, such interesting approaches as multidye thin-film LSCs [5, 10], photonic band filters and reflectors inside the LSCs [11-13], plasmonically-enhanced LSCs [14, 15], *etc.* were proposed.

With appearance of new materials, including metal oxides and rare earth element-doped glasses and polymers, exotic carbon based light-harvesting antennas, bio materials (see extensive reviews [10, 16] and

references thereof), and especially quantum dots (QDs) [17], the LSCs were revitalized and reevaluated. Colloidal QDs became very attractive candidates for the luminescent moieties in LSCs in regard to their stability, broad and high absorption, large Stokes-shifts reducing parasitic self-absorption [18]. Most of the research up to date was based on II–VI QDs and quantum rods (mainly CdSe-based [19]) due to the well-developed synthetic protocols, deeply studied physical and chemical properties and excellent photoluminescence (PL) quantum yield (QY) [20]. To overcome the limitations of high reabsorption losses of II-VI QDs, Stokes-shift engineering approaches were reported, including formation of giant shell around CdSe core [21, 22] or changing the luminescence mechanism by doping with metal ions [23]. As shown by Kennedy *et al.,* NIR emitting II-VI QDs can sufficiently improve the efficiency of the QDs-based LSCs [24]. During the last decade I-III-VI based QDs, such as $CuInS_2$ became very attractive alternative materials [25] replacing Cd-based QDs especially in LEDs [26, 27], solar light harvesting applications [28, 29] and bio-imaging [30]. In fact, the state-of-the-art I-III-VI QDs possess very large Stokes shifts (~400-500 meV) and high QYs approaching 0.8 in solution [31], and are flexible in spectral shifting due to the possibility to tune their composition. These give excellent prospects for achieving a PLQY for QDs embedded in transparent matrices of 0.5 and higher in the near future.

Recently this class of low-toxic QDs was considered for the application in LSCs. In particular, Klimov et al. [29, 32] and Sumner et al. [33] provided extensive reports on the application of $CuIn(S_x,Se_{1-x})_2$-based QDs in LSCs, using both analytical and numerical mathematical modelling and presented corresponding prototype composite materials and devices. In particular, the authors concluded about the growing role of scattering losses with an increase of QD loading for small geometric gain and dominative high waveguide losses with the scale up of the device [33].

In our previous report for spectral converters it was shown that Zn-Cu-In-S (ZCIS) QDs can outcompete CdSe QDs owing to their larger Stokes-shifts and thus lower self-absorption losses [34]. Besides this, ZCIS is a potentially non-toxic material, which is very important for large-scale applications.

In parallel to LSCs, the harvesting of dissipative sunlight energy is viable through PV windows, which can be realized in the form of semitransparent LSCs without the back-reflector (Fig. 1 a). In contrast to LSCs, much less attention has been paid to PV windows. To our best knowledge, no special simulations were performed for such systems based on QDs. At the locations excessively illuminated by solar light, the

buildings equipped with semitransparent windows (or walls) could be a passive energy source. Moreover, it is of high importance for the high quality inside lighting conditions, that these windows are able to retain a natural spectrum (color) of transmitted light. Several concepts are proposed for this goal. One approach is the direct application of semitransparent PV cells [35], which however is still challenging in view of the high costs. Another idea is to develop UV and NIR light absorbers in dye sensitized solar cells which will transmit the visible light without distortion, proposed by Zhang *et al*. [36]. A similar physical effect (UV and NIR light absorption) but different harvesting concept was reported by Zhao *et al.* [37]. The authors managed to create fully transparent and energy producing windows by the concept of planar solar concentration, previously reported *e.g.* in [38]. In the completely transparent device of Zhao *et al.* molecules absorb small portions of invisible UV light and reemit this energy as a secondary light at longer wavelengths being partially guided to the edges by total internal reflection. At the edges, thin strips of conventional silicon-based solar cells are attached. However, it is highly desirable to extend the range of the absorbed light. From this perspective, the appearance of colloidal QDs granted this possibility ensuring in addition a better long-term stability.

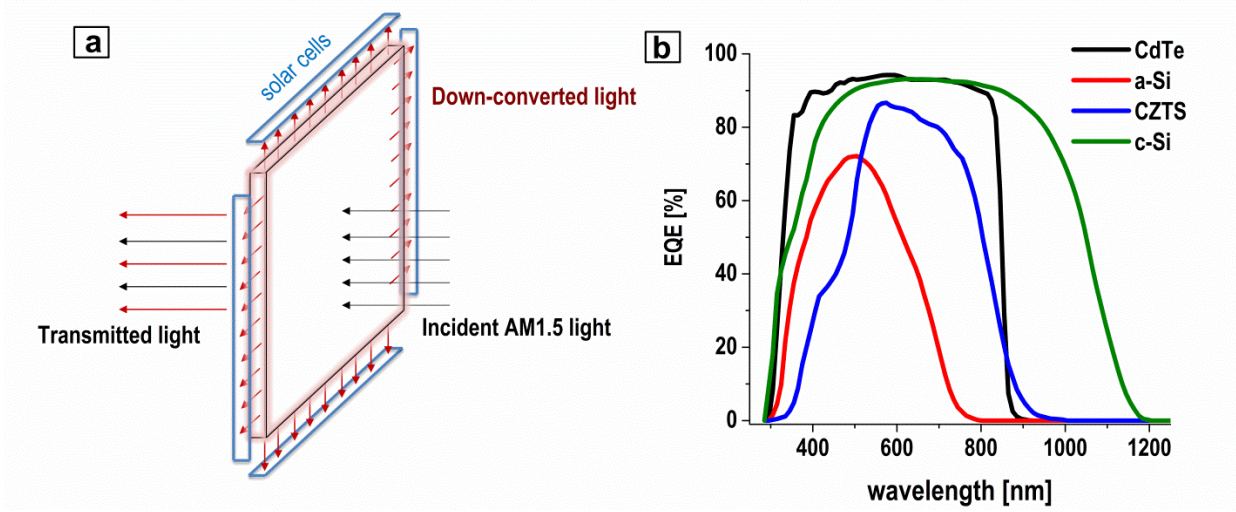

Fig. 1. (a) Schematic representation of the modeled PV window prototype. Solar cells are placed along the perimeter of the down converting plate. (b) External quantum efficiencies of solar cells considered as photovoltaic elements in our calculations. The data for c-Si are measured by ourselves, those for a-Si, CZTS and CdTe cells adopted from references [39-41], respectively.

Recently, we developed a procedure for the fabrication of QDs-in-polymer composite materials suitable for large scale samples with controllable particle load through the QDs surface-engineering and co-polymerization process [42]. In present work we adopted experimental knowledge and the characterization results from the above mentioned paper to analyze the feasibility of $CuInS_2$ (CIS)-based composites with different QYs and geometries for application in PV windows by Monte-Carlo simulations. Furthermore, we performed a quantitative assessment of the power generation potential of this technology for two levels of average transparency in the visible optical range (90% and 70%) and analyzed the spectral content of the transmitted light through the PV window prototype.

The Monte-Carlo or ray-tracing approach [9, 43-45] consists in the calculation of a single photon path through the PV window with possibilities to be transferred according to ray optics, *i.e.* to be absorbed, emitted, reabsorbed, reflected from the interface and refracted to the outer medium. Each of these processes has a certain probability, calculated with the program. The ray interactions with interfaces are described with the Fresnel equation for the unpolarized light taking to account the incidence angle and refractive indexes of the media. After the reflection coefficient *R* for the current ray (photon) is calculated (from 0 to 1) the uniformly distributed random value within [0,1] is generated and compared with the *R* to make the decision about reflection or transmission event. To trace the photon through the medium, the one-shot path is generated as a function of a random number and ~~then~~ the extinction coefficient (see [34, 43]). This path is compared with the distance to the ~~plane~~ interface in the direction of the photon, and the decision about the absorption or intersection with the interface is made. If the photon is absorbed, the emission probability is sampled similarly using the quantum yield value. The wavelength of the new emitted photon is assigned according to the normal distribution of the spectrum with the predefined central wavelength. The model takes to account the experimentally observed spectrum broadening at longer wavelengths.

~~which defines the absorption, reflection or refraction event.~~ After the photon tracing is completed, the final light flux profile (spectrum) $\phi(\lambda)$ at the edges and behind the window can be collected. The short circuit current can be calculated as an integral value of photons (converted to free carriers) in respect to the external quantum efficiency (EQE) curve of a solar cell according to the following well known equation:

$$J_{sc} = q \int_{\lambda_1}^{\lambda_1} \phi(\lambda) EQE(\lambda) d\lambda \qquad (1)$$

In our model, λ_1 and λ_2 correspond to 285 and 1250 nm, respectively.

As photovoltaic elements for the conversion of light transmitted to edges we consider exemplarily two silicon-based and two alternative thin-film solar cells which have industrial history and which are established technology or show promising stability. Important, they consist of abundant materials: mono-crystalline (c-Si) and amorphous silicon (a-Si) as most common outdoor and indoor solar cells, Cu_2ZnSnS_4 (CZTS) as environment-friendly and low-cost absorber and CdTe with the lowest energy pay-back time up-to date and little sensitivity to low-light conditions. At the present time, we cannot predict which of the new emerging technologies (organic, perovskite, dye-sensitized, QD-based *etc.* solar cells) will achieve stable characteristics and come to the large-scale market. In this respect we limit our consideration to the above mentioned well established solar cell technologies.

For the c-Si we use measured EQE characteristics of a commercially available cell. EQE characteristics for a-Si (glass/TCO/p-i-n a-Si:H/ZnO:Ag, without nanoparticles) were adapted from [39], for CZTS (IPCE above 8%) – from [40] and for CdTe – from [41]. Corresponding EQE curves are presented in the Fig. 1, b.

For the incident light spectrum we adopt the ASTM G173-03 (AM1.5G) spectrum from [46] with a normalized to 80 mW/cm^2 flux. Absorption and emission spectra of our experimentally available Zn-Cu-In-S QDs dispersed in polystyrene are represented in Fig. 2 (inset). These spectra are typical for CIS-based systems and possess large Stokes-shifts and reduced self-absorption in comparison to the most of the II-VI counterparts, *e.g.* CdSe/ZnS QDs.

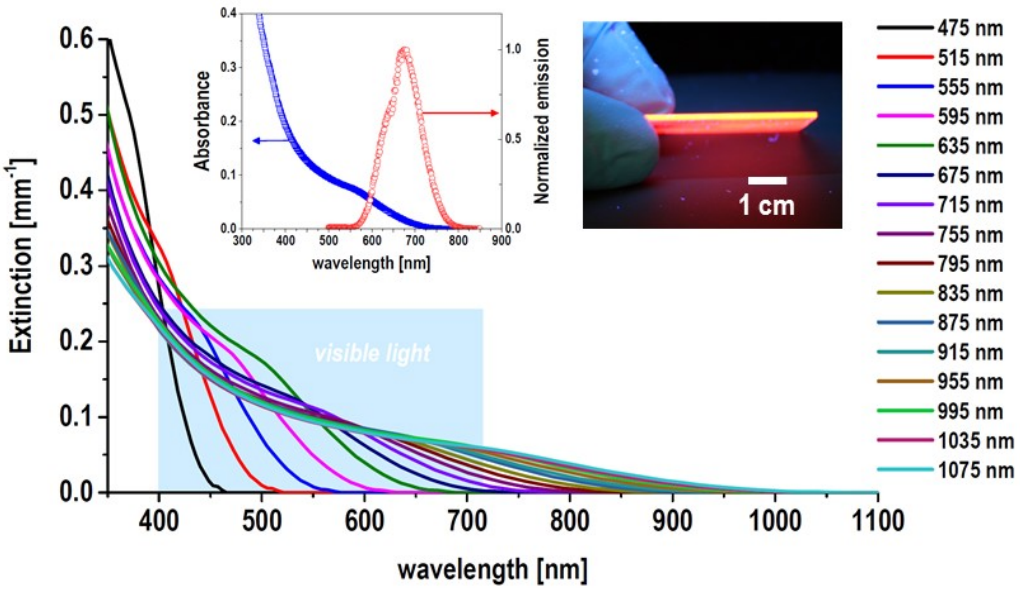

Fig. 2. Extinction spectra taken as an input parameter for different model QDs with emission maxima from 475 to 1075 nm. The average transmittance in the visible region remains constant (90 or 70% for presented simulations). Inset left: Typical experimental emission and absorption spectra of Zn-Cu-In-S QDs in polystyrene, fabricated in our laboratory. Inset right: optical image of luminescent composite UV light fabricated through the surface engineering approach (ZCIS/ZnS QDs in polystyrene) for potential application in PV windows.

The input absorption and emission parameters for different QDs were created as a set of spectra based on experimentally observed shape profile (emission maximum at 675 nm and absorption shoulder at 545 nm), but with gradual shift of both absorption and emission corresponding to the emission maximum covering a range of interest between 475 to 1095 nm. For each spectral profile the Stokes-shift, which was acquired from experimental curves (~440 meV), is retained. For example, as mentioned above, to the emission spectrum with the maximum at 675 nm corresponds the absorption curve with first excitonic shoulder at ~545 nm, for the PL maximum at 995 nm – the excitonic shoulder at 740 nm. The absorption curves were further normalized in such a way, that the average optical transmittance T of the prototype in the range of the human eye sensitivity (400–730 nm) remains nearly constant (we chose two cases T=0.7 or T=0.9). These spectral changes are shown in Fig. 2 (main graph) and correspond to the typically observed changes in size and composition of CIS-based QDs [31]. Through this spectral design we are able to define the optimal spectral profile for each solar cell and study the impact of spectral properties of the PV window

prototype on the light flux which passes the PV window and which appears for the consumer as slightly shadowy but realistically colored day light behind the window. We define the optimal spectral profile as the one which appears nearly colorless.

For every emission profile, the short circuit current for solar cells at the four edges of a 100 mmx100 mm PV window prototype can be calculated. Based on the open circuit voltage (V_{oc}) and the fill factor (FF), the maximal power can be evaluated. In our simulations we consider different aspect ratios of the lateral dimensions, the thickness of the PV window and its influence on the overall efficiency. By the power evaluation we note, that the V_{oc} depends on the short circuit current I_{SC} ($V_{oc} \propto \frac{kT}{q} ln\left(\frac{I_{sc}+I_s}{I_s}\right)$), and due to the shunt-resistance effect, the overall efficiency of the cell in general decreases at low-light conditions. For simplicity, in the present study we assume that the short circuit scales strictly linear with the light flux, that means $I_{sc}[\frac{1}{x} Sun]=\frac{1}{x} I_{sc}[1\ Sun]$ for 1<x<10, and only V_{oc} and FF are affected by low light conditions. The excitation and emission kinetics of the QDs is simplified here. We do not introduce the "off" state and assume that the luminescent intensity has a linear response under sun illumination and is reflected in the average QY. QY values are iterated from 0.1 to 0.9 (we note, that QY=1 for colloidal QDs embedded in a polymer is in practice hardly achievable). State-of-the-art value of 0.5 has been reported [21] and taken here as a reasonable average value).

The photons which are not wave-guided to the edges by the total internal reflection (referred usually as 'cone losses') are traced by the model until they refract from the PV window. Before they do this, they can be reabsorbed/reemitted and contribute to the short current (at the edges) or refract through the top or front interfaces and contribute to color of the PV window. This feature of the model makes it more correct in comparison with the analytical models where the 'cone losses' are ignored.

The interface between QDs containing composite and the solar cell is modelled without an antireflective coating. Scattering and absorption losses in the matrix are considered as negligible. Incident photons are traced normally to the front surface.

Results and discussion.

In the PV window a spectral conversion process (down-shifting) occurs. This process guides the light to the edges, which is strongly dependent on the QY of the embedded QDs (Fig. 3). PV windows with constant transmittance in the visible region can transfer more energy, if luminescent particles emit at longer wavelengths (*e.g.* in the NIR), since the light of a broader spectral range is absorbed (visible and additionally a part of the NIR, as can be seen in Fig. 2). The reduction of the transmittance from 90 to 70% causes the guided power to increase by a factor of 2.5 for QDs emitting at ~700 nm, and by a factor of 3 for wavelengths λ>910 nm for a QY=0.5. For example, for normal incidence of 80 mW/cm^2 AM 1.5 solar irradiation, a modeled prototype with a surface of 100 mm x 100 mm and a thickness of 1 mm can transfer 22 mW of power to the edges with T=90% and QY=0.1, nearly 115 mW with T=90% and QY=0.5, and 260 mW with T=70% and QY=0.5.

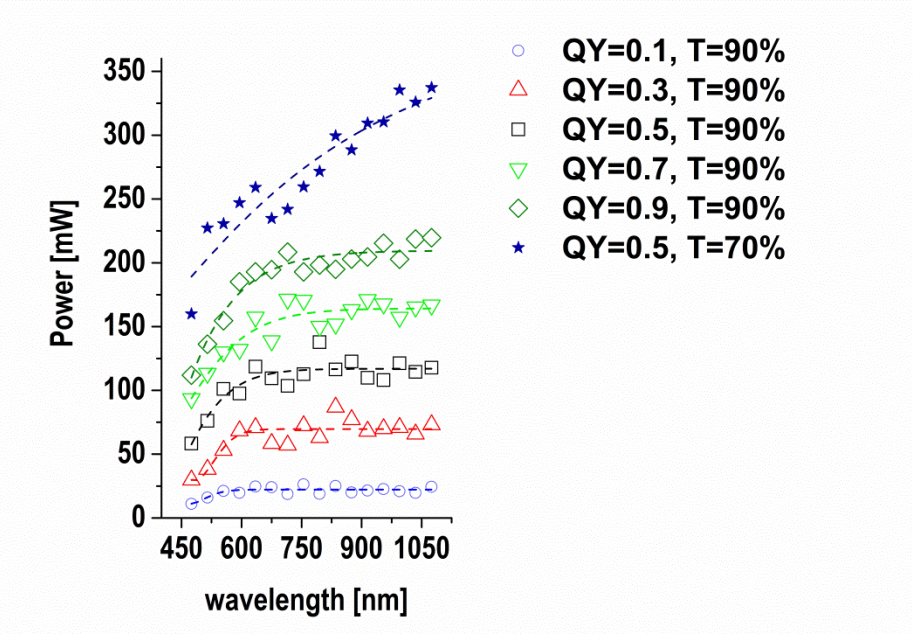

Fig. 3. Power transferred to the edges of the modelled PV window prototype (100x100x1 mm^3) with CIS-based QDs having varied emission wavelengths and a transmittance of 90% and 70%, as a function of the QDs emission spectrum. Device is illuminated by the 80 mW/cm^2 sun flux (AM1.5). Stars denote a transferred power in case of 70% transmittance of the PV window.

In Fig. 4, the curves of the short circuit current as a function of the maximum emission wavelength of the QDs are presented for CdTe, c-Si, a-Si and CZTS edge solar cells. The aspect ratio for the modeled PV window was chosen to be 0.01 (1 mm thickness, 100x100 mm^2 front surface) for this simulation, which corresponds to the geometric gain G=25 (defined as a ratio between the front surface area and the area of four edges, $G = \frac{S_{front}}{S_{edges}}$). Dotted graphs in Fig. 4 contain dispersion, which comes from the precision error of our Monte-Carlo method, but the main tendencies can be clearly followed. Due to the wide spectral range of high conversion efficiency, c-Si shows superiority over thin-film solar cells. However, due to the distinct dependence of V_{oc} and *FF* on the light flux, this advantage may vanish under real conditions. For the c-Si solar cell, an optimal spectral range for the QD emission lies between 875 and 955 nm, for CdTe and CZTS it is 675-755 nm, for a-Si – 555–595 nm. As can be seen, I_{sc} strongly depends on the QY. In Fig. 5 these dependencies are summarized for 90 and 70% of PV window transmittances for 100×100×1 mm^3 dimensions. The simulations were performed for each solar cell with corresponding optimal central emission wavelengths.

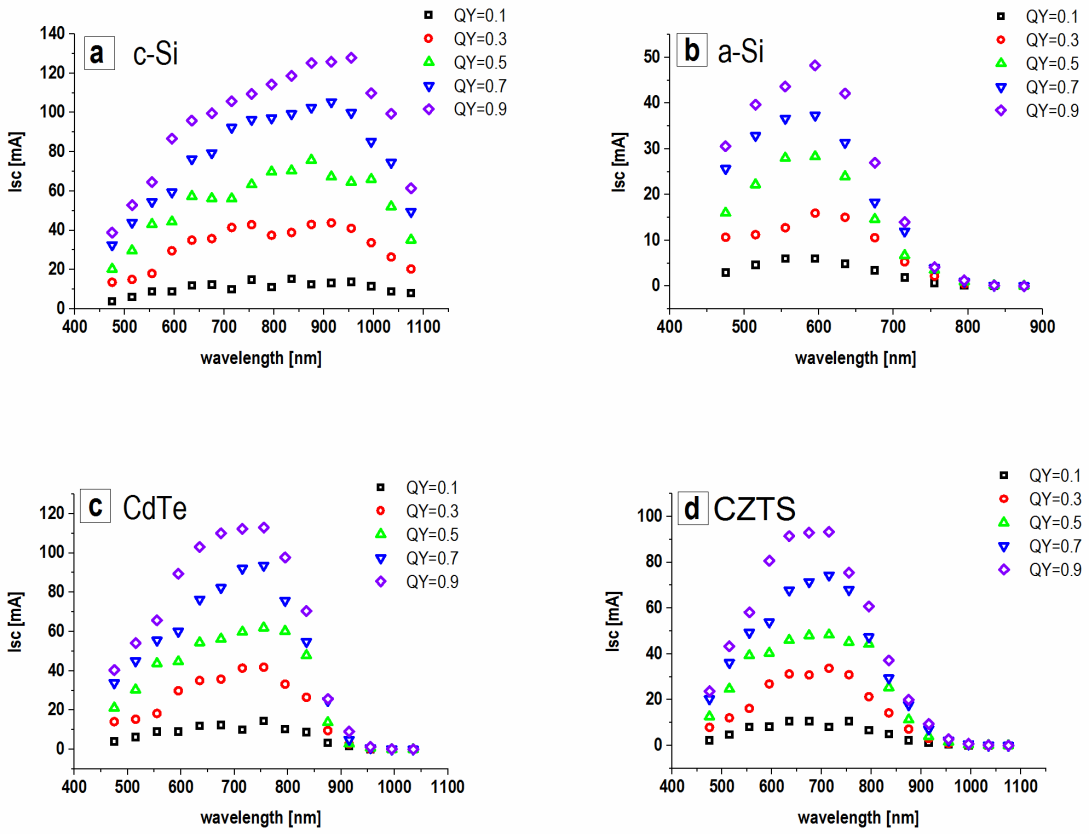

Fig. 4. Short circuit current of the solar cells at the edges as a function of QD PL spectrum in the PV window prototype (the wavelength represents the central emission wavelength): c-Si (a), a-Si (b), CdTe (c) and CZTS (d) (incident AM1.5 solar spectrum with light flux density 80 mW/cm^2, transmittance of the PV window set to 0.9).

We note the linear dependency of the current on the QY (Fig. 5 a, b). Since the simulations were performed for different spectral profiles for each solar cell (with optimal to each one), the increase in I_{sc} upon change from 90% to 70% transmittance differs. It is the most pronounced for c-Si solar cell (by factor 2.8), for other solar cells the photocurrent increases by a factor of 2.17–2.25. This behavior for c-Si solar cell can be explained by its best performance in the NIR spectral region. According to our simulation method, we used the spectral profile for the central emission wavelength 915 nm. To keep the transmittance constant at 70%, the absorption in the blue range was reduced, but in the red range and the NIR increased. In the latter region, the integral amount of photons is higher, thus the overall increase in I_{sc} for c-Si solar cell is steeper (Fig. 5, b).

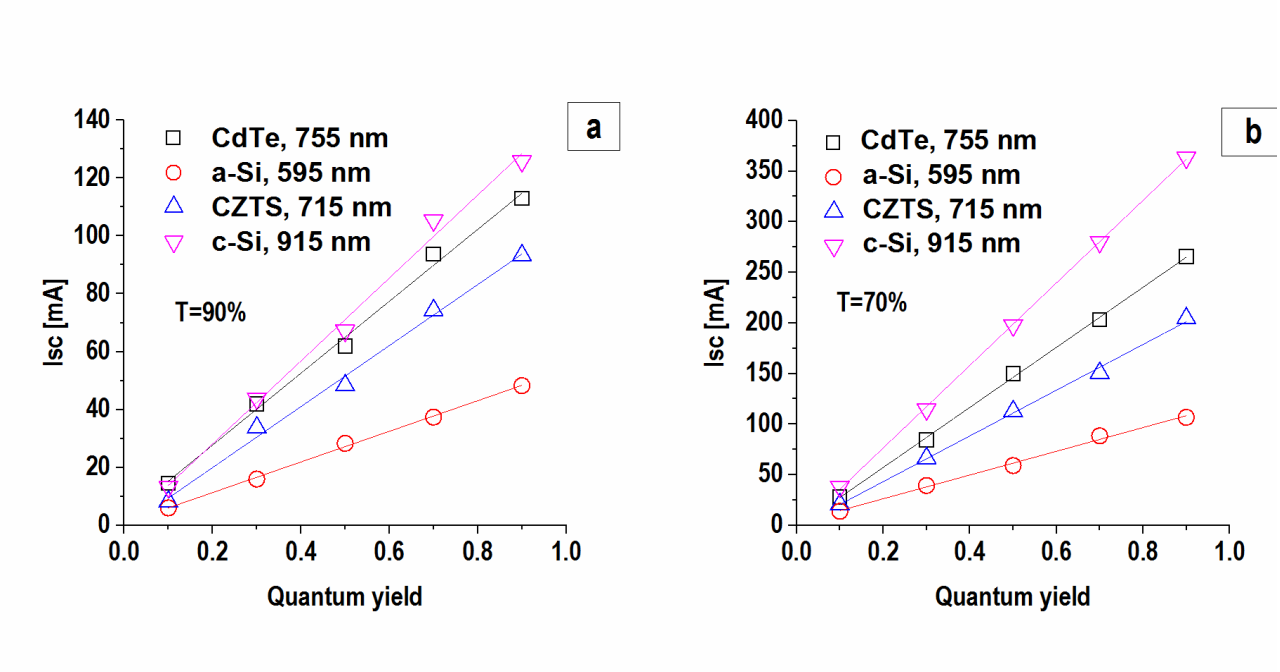

Fig. 5. Photocurrent of the edge SCs as a function of quantum yield for PV window prototype with surface area of 100×100 mm^2 , thickness 1 mm, geometric gain G= 25 (incident spectrum AM1.5, 80 mW/cm^2). The data provided for transmittances of 90% (a) and 70% (b), respectively.

Along with the influence of the QD spectral properties on the performance of the PV window, the geometry of the device alters the output. On the one hand, an increase in the aspect ratio (understood as increase in thickness of the PV window by constant front area) and correspondingly decrease of geometric gain provide edges with more photons able to reach them with less reflection events at the front and back interface. Thus more power can be transferred and harvested. At lower G the current in the solar cell reaches saturation. This is shown exemplarily for the c-Si based PV window in Fig. 6 a. On the other hand, an increase of the device thickness influences the concentration effect of the PV window, thus we observe a decrease of the power concentration factor (c-factor, defined as a ratio of flux densities incident onto edges and front surface, Fig. 6 b). In this case the efficiency decrease of a solar cell is expected. For example, an increase of the aspect ratio from 0.01 to 0.02 will boost the photocurrent by 50%. At the same time, the c-factor will decrease nearly from 0.8 to 0.6 for QDs with a central emission wavelength of 755 nm and a QY of 0.5. We refer to the low-light conditions effect study on the solar cells performance of Randall *et al.* [47]. Based on the data for several c-Si solar cells and modules, we note that the efficiency should not decrease more than by 2.5% for the c-factor drop from 0.8 to 0.6. Thereby, thicker windows would be beneficial

from a point of view of their performance. However, the design, mass and the price of the matrix (*e.g.* polymer, glass) may be an essential restrictive factor. To our knowledge, for the large scale mass-production applications the aspect ratio of more than 0.01 is unlikely (*e.g.* 1 cm at 1 m^2 surface area), thus we adopt this value as a standard for further considerations. The c-factor dependency on the geometric gain in Fig. 6 b shows initial quasilinear increase (defined by geometry) with further saturation defined by the waveguide losses. This behavior is consistent with analytical models of LSCs [32] and primarily comes from thermodynamic restrictions for the concentration for every luminescent moiety. Additionally we note, that at given conditions (Fig. 6 b), the c-factor can exceed unity if the QY of QDs containing composite material will reach 0.7.

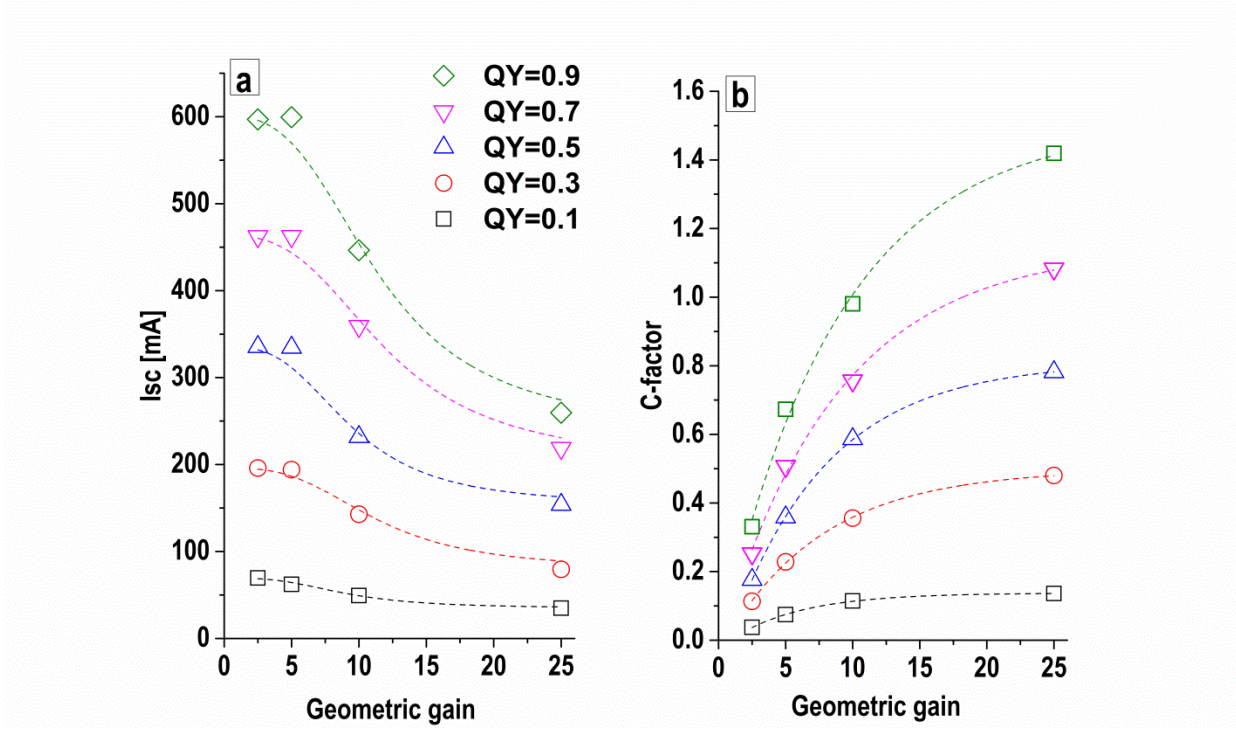

Fig. 6. Photocurrent of a c-Si solar cell at the edges of a PV window prototype as a function of varying geometric gain *G* (for 100x100 mm^2 surface area) at constant emission and absorption profile of CIS QDs ($\lambda_{emission}$=755 nm, under AM1.5, 80 mW/cm^2 illumination, transmittance of the PV window = 70%). QY varies in the range of 0.1–0.9.

For the future consumers of PV windows, the transmitted light spectrum is of high importance. The Monte-Carlo tracing is a convenient instrument to study the changes of the spectrum of transmitted light behind the window, in combination with the chromaticity diagram. Again, we gradually shifted the

spectral profile of the QDs inside the modeled window and collected the output spectrum, shown in Fig. 7. Furthermore, based on the spectra (converted to power per area) the CIE[1]1931 coordinates were calculated.

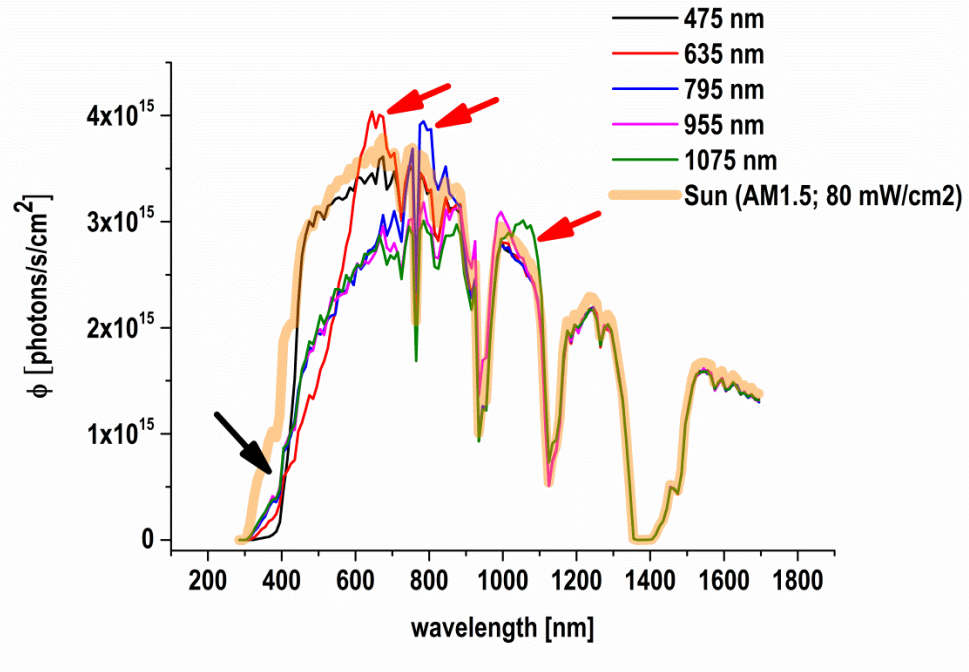

Fig. 7. Spectra of transmitted light through the PV window prototype (aspect ratio = 0.01, *G*=25, average transmittance = 70%) with varying spectral properties of the QDs. Exemplarily, the spectra for luminescent particles which emit with QY=0.5 at λ_{max}=475 nm, 635 nm, 795 nm, 955 nm, 1075 nm are shown. Thick line is the AM 1.5G Sun spectrum (80 mW/cm^2).

The modification of the transmitted spectrum and the appearance of the window color are caused on the one hand by a high absorption coefficient of the QDs at shorter wavelengths (black arrow, Fig. 7), and appearing QDs emission through the "escape cone" on the other hand (red arrows). Thus, the incident white light can be essentially shifted to green, brown or red tones. The evolution of chromaticity coordinates is shown in Fig. 8. The points in the diagram follow an ellipse-like curve. We note that the QDs which emit in the spectral region 515–675 nm contribute to an appearance of the color. The closest to the white light in the color space are points which correspond to λ>795 nm. The spectrum in the Fig. 7, which corresponds to 475 nm central emission wavelength, provides too low system efficiency, and cannot be considered for

[1] International Commission on Illumination

potential application. If we combine these findings with analysis of the data shown in Fig. 4, we can conclude, that to keep the PV window colorless and to ensure high efficiency of the device, we should use the QDs emitting at λ>795 nm in combination with the silicon edge solar cell or the solar cell with similar spectral properties.

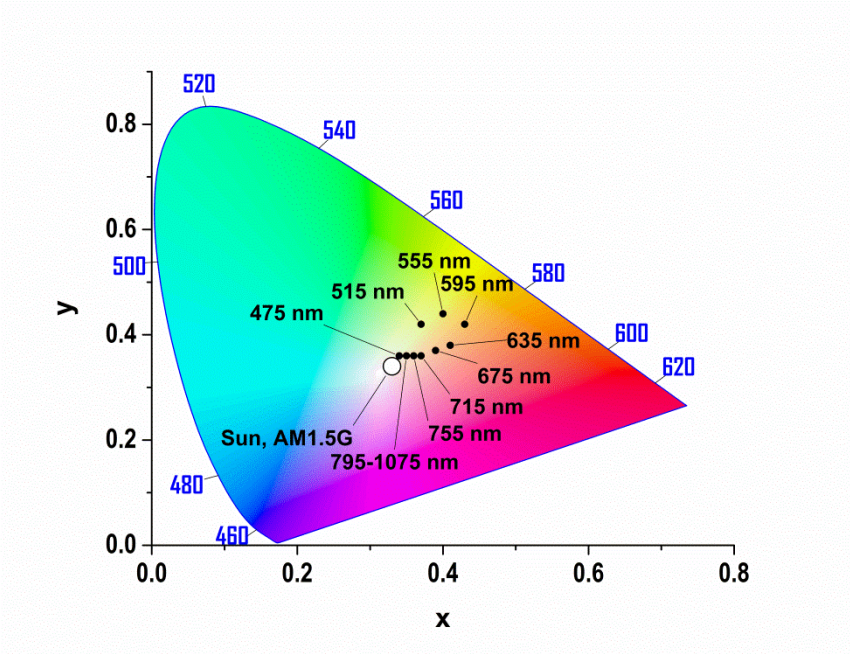

Fig. 8. Positions of the transmitted spectra through a simulated PV window on the Chromaticity diagram (*CIE1931*), shown exemplarily for following conditions: aspect ratio = 0.01, average transmittance = 70%, QY=0.5.

It should be noted, that CIS/ZnS or ZCIS/ZnS QDs do not exhibit luminescence in the NIR spectral region, being in a strong quantum confinement. The bulk energy gap of 1.53 eV can be increased up to 2 eV and further, causing the emission in the spectral region of 600–700 nm. An example is shown in Fig. 2 (right inset). To achieve further emission shifts to the NIR, the CIS nanocrystals can be doped/alloyed with selenium, as reported by Meinardi *et al.* [29].

Based on the obtained data for four solar cells, we evaluate the maximum power which can be generated by a CIS-based PV window prototype, according to the expression $P_{max} = FF \cdot I_{sc} \cdot V_{oc} \cdot \beta$. For the efficiency change under low light conditions we introduce the correction factor β, adapted from literature. β reflects the consolidated efficiency change under low illumination conditions, contributed both by FF and V_{oc}. The short circuit current I_{sc} comes from our simulations for QY=0.5; c-factor = 0.78 for the

aspect ratio = 0.01, *G*=25, and FF and V_{oc} taken from the literature for each cell. We note, that in an ideal case CdTe solar cells attached to the edges of an 100x100 mm^2 PV window can produce ≈41 mW at T=90% and ≈95 mW at T=70% with the QY=0.5 (by 80 mW/cm^2 incident AM1.5 spectrum). The power almost doubles with the QY of 0.9. The values of c-Si correspond to 34 and 85 mW (QY=0.5); 58 and 163 mW (QY=0.9). Although the values of CdTe and c-Si lie close to each other, CdTe solar cells shows better performance. One reason lies in the input data – we use a CdTe EQE curve adapted from literature for a cell, but for the complete module I_{sc}, V_{oc} and FF may slightly differ (decrease). For the c-Si we use a measured EQE curve of a commercially available cell. Another reason is in the different QDs, which should be used for different systems. For the CdTe system, the best performance can be achieved with the QDs which emit close to 700 nm. However, as discussed, the corresponding spectral profile of the QDs will introduce a color tone for the PV window. For the c-Si the optimal region is 875–955 nm. Along with the emission, in our method the absorption spectra are changed (see Fig. 2 and method description), which may result in slightly more favorable conditions for CdTe solar cell. The third reason is the high V_{oc} and optimized EQE of CdTe cells, which provide better power conversion. CZTS and a-Si solar cells would produce essentially lower amounts of energy. Another drawback of the a-Si solar cell is the poor spectral matching, if the condition of colorless PV window would be fulfilled.

To evaluate the overall system performance for modelled prototype, the optical efficiency η for different system parameters were calculated, presented in *Table 1* ($\eta=P_{produced}/P_{incident}$). For maximal produced power, P_{max} at QY=0.9 the concentration factor exceeds 1 and is close to 1.4, which should cause an increase of the cell efficiency for most semiconductor solar cells, but may worsen the solar cell long time performance, especially for systems with a-Si absorber [48]. We find that optimized systems for c-Si or CdTe solar cells could have optical efficiencies exceeding 2% in 70% transparent windows, which is promising for future applications. As discussed in the literature, the self-absorption effect in solar concentrators and PV windows can sufficiently suppress the system performance [19, 29, 33]. In the case of CIS or ZCIS QDs, this detrimental effect is sufficiently reduced (but not eliminated) due to the large Stokes-shift, in comparison to CdSe/ZnS core-shell QDs [25]. However, for the 100x100 mm^2 window the self-absorption still reduces the energy transfer approx. by factor 1.1–1.7 for QY=0.5 depending on the spectral emission-absorption profile of given particles and the QY (from our experience, the absorption overlap is

higher in the blue region and decreases toward the NIR). To scale up the modelled device experimentally to 1 m^2, sufficient efforts should be done in overcoming the waveguide parasitic losses, first of all due to the solving of the QY suppression problem in fabrication of luminescent composites.

Table 1. *Calculated maximal power and optical efficiency of the modelled prototype PV window for four solar cells and QY=0.5 and 0.9. For each system (QDs+solar cells) the optimal conditions in respect to generated power were considered.*

Solar cell	I_{sc} [mA]	V_{oc} [V]	FF	β	P_{max} [mW] QY=0.5	P_{max} [mW] QY=0.9
CdTe	62 (T=90%) 143 (T=70%)	0.85 V	0.78	≥1	41.1 (η=0.5%) 94.6 (η=1.2%)	> 75 (η=0.94%) > 176 (η=2.2%)
CZTS	48 (T=90%) 103 (T=70%)	0.66 V	0.65	1*	20.6 (η=0.26%) 44 (η=0.55%)	> 41 (η=0.5%) > 89 (η=1.1%)
c-Si	76 (T=90%) 190 (T=70%)	0.6 V	0.76	0.98	33.9 (η=0.42%) 85.1 (η=1.1%)	> 58 (η=0.73%) > 163 (η=2.1%)
a-Si	28 (T=90%) 64 (T=70%)	0.81 V	0.47	≥1	10.7 (η=0.13%) 24.4 (η=0.3%)	> 18 (η=0.5%) > 40 (η=0.5%)

* **no data found for CZTS performance at low light conditions**

Conclusions

In conclusion, we assessed the potential application of $CuInS_2$ based QDs in photovoltaic windows – a passive source of clean energy for building integrated technologies. By means of Monte-Carlo ray tracing simulations we defined optimal spectral regions of the QDs emission for c-Si, a-Si, CdTe and CZTS solar cells at the edges of a potentially non-toxic PV window prototype. We analyzed the influence of window transmittance, QDs quantum yield and window geometry on the photocurrent and the power of the simulated device on the base of spectral profiles of $CuInS_2$ QDs obtained by colloidal synthesis. Our calculations showed that the power produced by a 100x100 mm^2 CIS QDs based PV window prototype can reach values of 85–95 mW with an optical performance of the system of 1.1–1.2% assuming a QY of 0.5 and 70% average transmittance in the visible region, that can be increased up to 175 mW (2.2% optical performance), if the QY reaches 0.9 (incident AM1.5G 80 mW/cm^2 Sun spectrum). The design of the PV window should fulfill the compromise between the tendencies to increased thickness (increases the photoresponse) and decrease of the concentration factor (reduces the efficiency of the solar cell). By transferring the transmitted spectrum to color space we defined the color of the light behind the window (delivered to consumer) and found that the QD with emission maximum at λ>795 nm provide inside

illumination conditions closest to the white light point. This imposes restrictions on the choice of appropriate solar cells, attached to the edges. We found the c-Si solar cell as optimal choice for this purpose. Finally, the results showed that the modeled PV windows can be a useful passive energy source. The vital condition is the improvement of the QY of semitransparent composite materials based on QDs in specified spectral regions.

Notes

The authors declare no completing financial interest.

Conflict of interest

There are no conflicts to declare.

Acknowledgements

RL and NG acknowledge Dresden Fellowship Program 2016 under grant agreement F003661-553-61D-1716100. This work was supported by ERC Starting Grant "2D-SYNETRA" – Seventh Framework Program FP7, Project: 304980 (Simulations).

References

1. *BP Statistical Review of World Energy, June 2016.* www.bp.com/statisticalreview.
2. *Photovoltaics Report. Fraunhofer Institute for Solar Energy Systems, ISE. November 2016.* www.ise.fraunhofer.de.
3. *Renewables 2016. Global Status Report. REN21.* www.ren21.net, Report ISBN 978-3-9818107-0-7.
4. W. Weber and J. Lambe, *Appl. Opt.*, 1976, **15**, 2299-2300.
5. A. Goetzberger and W. Greube, *Appl. Phys. A Mater. Sci. Process.*, 1977, **14**, 123-139.
6. J. Batchelder, A. Zewail and T. Cole, *Appl. Opt.*, 1981, **20**, 3733-3754.
7. C. L. Mulder, P. D. Reusswig, A. Beyler, H. Kim, C. Rotschild and M. Baldo, *Opt. Express*, 2010, **18**, A91-A99.
8. M. S. de Cardona, M. Carrascosa, F. Meseguer, F. Cusso and F. Jaque, *Appl. Opt.*, 1985, **24**, 2028-2032.
9. L. H. Slooff, E. E. Bende, A. R. Burgers, T. Budel, M. Pravettoni, R. P. Kenny, E. D. Dunlop and A. Büchtemann, *Phys. Status Solidi - Rap. Res. Lett.*, 2008, **2**, 257-259.
10. B. C. Rowan, L. R. Wilson and B. S. Richards, *IEEE J. Sel. Topics Quantum Electron.*, 2008, **14**, 1312-1322.
11. J. C. Goldschmidt, M. Peters, A. Bösch, H. Helmers, F. Dimroth, S. W. Glunz and G. Willeke, *Sol. Energy Mater. Sol. Cells*, 2009, **93**, 176-182.
12. R. Reisfeld, *Opt. Mater.*, 2010, **32**, 850-856.
13. L. Xu, Y. Yao, N. D. Bronstein, L. Li, A. P. Alivisatos and R. G. Nuzzo, *ACS Photonics*, 2016, **3**, 278-285.
14. S. Chandra, J. Doran, S. McCormack, M. Kennedy and A. Chatten, *Sol. Energy Mater. Sol. Cells*, 2012, **98**, 385-390.
15. M. G. Debije and P. P. Verbunt, *Adv. Energy Mater.*, 2012, **2**, 12-35.
16. F. Purcell-Milton and Y. K. Gun'ko, *J. Mater. Chem.*, 2012, **22**, 16687-16697.
17. W. G. van Sark, K. W. Barnham, L. H. Slooff, A. J. Chatten, A. Büchtemann, A. Meyer, S. J. McCormack, R. Koole, D. J. Farrell and R. Bose, *Opt. Express*, 2008, **16**, 21773-21792.
18. S. Gallagher, B. Rowan, J. Doran and B. Norton, *Solar Energy*, 2007, **81**, 540-547.
19. J. Bomm, A. Büchtemann, A. Fiore, L. Manna, J. H. Nelson, D. Hill and W. G. van Sark, *Beilstein J. Nanotechnol.*, 2010, **1**, 94-100.
20. P. Reiss, J. Bleuse and A. Pron, *Nano Lett.*, 2002, **2**, 781-784.
21. F. Meinardi, A. Colombo, K. A. Velizhanin, R. Simonutti, M. Lorenzon, L. Beverina, R. Viswanatha, V. I. Klimov and S. Brovelli, *Nat. Photonics*, 2014, **8**, 392-399.
22. I. Coropceanu and M. G. Bawendi, *Nano Lett.*, 2014, **14**, 4097-4101.
23. C. S. Erickson, L. R. Bradshaw, S. McDowall, J. D. Gilbertson, D. R. Gamelin and D. L. Patrick, *ACS nano*, 2014, **8**, 3461-3467.
24. M . Kennedy, S . McCormack, J . Doran, B. Norton, *Sol. Energy* 2009, 83(7):978-81.
25. K. E. Knowles, K. H. Hartstein, T. B. Kilburn, A. Marchioro, H. D. Nelson, P. J. Whitham and D. R. Gamelin, *Chem. Rev.*, 2016, **116**, 10820-10851.
26. P. Ilaiyaraja, P. S. Mocherla, T. K. Srinivasan and C. Sudakar, *ACS Appl. Mater. Interfaces*, 2016, **8**, 12456-12465.
27. J. Zhang, R. Xie and W. Yang, *Chem. Mater.*, 2011, **23**, 3357-3361.

28. H. McDaniel, A. Y. Koposov, S. Draguta, N. S. Makarov, J. M. Pietryga and V. I. Klimov, *J. Phys. Chem. C*, 2014, **118**, 16987-16994.
29. F. Meinardi, H. McDaniel, F. Carulli, A. Colombo, K. A. Velizhanin, N. S. Makarov, R. Simonutti, V. I. Klimov and S. Brovelli, *Nat. Nanotech.*, 2015.
30. W. Guo, N. Chen, C. Dong, Y. Tu, J. Chang and B. Zhang, *Rsc Advances*, 2013, **3**, 9470-9475.
31. P.-H. Chuang, C. C. Lin and R.-S. Liu, *ACS Appl. Mater. Interfaces*, 2014, **6**, 15379-15387.
32. V. I. Klimov, T. A. Baker, J. Lim, K. A. Velizhanin and H. McDaniel, *ACS Photonics*, 2016, **3**, 1138-1148.
33. R. Sumner, S. Eiselt, T. B. Kilburn, C. Erickson, B. Carlson, D. R. Gamelin, S. McDowall and D. L. Patrick, *J. Phys. Chem. C*, 2017.
34. R. Lesyuk, V. Marinov, E. K. Hobbie, A. Elbaradei, I. Tarnavchyk and Y. Bobitski, *Sol. Energy Mater. Sol. Cells*, 2016, **151**, 52-59.
35. J. Ajuria, I. Etxebarria, W. Cambarau, U. Muñecas, R. Tena-Zaera, J. C. Jimeno and R. Pacios, *Energy Environ. Sci.*, 2011, **4**, 453-458.
36. K. Zhang, C. Qin, X. Yang, A. Islam, S. Zhang, H. Chen and L. Han, *Adv. Energy Mater.*, 2014, **4**.
37. Y. Zhao, G. A. Meek, B. G. Levine and R. R. Lunt, *Adv. Opt. Mater.*, 2014, **2**, 606-611.
38. M. J. Currie, J. K. Mapel, T. D. Heidel, S. Goffri and M. A. Baldo, *Science*, 2008, **321**, 226-228.
39. X. Chen, B. Jia, J. K. Saha, B. Cai, N. Stokes, Q. Qiao, Y. Wang, Z. Shi and M. Gu, *Nano Lett.*, 2012, **12**, 2187-2192.
40. B. Shin, O. Gunawan, Y. Zhu, N. A. Bojarczuk, S. J. Chey and S. Guha, *Prog. Photovolt. Res. Appl.*, 2013, **21**, 72-76.
41. M. Gloeckler, I. Sankin and Z. Zhao, *IEEE J. Photovolt.*, 2013, **3**, 1389-1393.
42. R. Lesyuk, B. Cai, U. Reuter, N. Gaponik, D. Popovych and V. Lesnyak, *Small Methods (DOI: 10.1002/smtd.201700189)*.
43. S. A. Prahl, M. Keijzer, S. L. Jacques and A. J. Welch, *Dosimetry of laser radiation in medicine and biology*, 1989, **5**, 102-111.
44. B. Richards and K. McIntosh, *Prog. Photovolt. Res. Appl.*, 2007, **15**, 27-34.
45. A. Kerrouche, D. Hardy, D. Ross and B. Richards, *Sol. Energy Mater. Sol. Cells*, 2014, **122**, 99-106.
46. http://rredc.nrel.gov/.
47. J. Randall and J. Jacot, *Ren. Energy*, 2003, **28**, 1851-1864.
48. R. Rüther and J. Livingstone, *Sol. Energy Mater. Sol. Cells*, 1995, **36**, 29-43.